Accepted Manuscript

Solvothermal hot injection synthesis of core-shell AgNi nanoparticles

Vit Vykoukal, Jiri Bursik, Pavla Roupcova, David A. Cullen, Jiri Pinkas

PII: S0925-8388(18)32955-4

DOI: 10.1016/j.jallcom.2018.08.082

Reference: JALCOM 47170

To appear in: *Journal of Alloys and Compounds*

Received Date: 22 May 2018

Revised Date: 6 August 2018

Accepted Date: 9 August 2018

Please cite this article as: V. Vykoukal, J. Bursik, P. Roupcova, D.A. Cullen, J. Pinkas, Solvothermal hot injection synthesis of core-shell AgNi nanoparticles, *Journal of Alloys and Compounds* (2018), doi: 10.1016/j.jallcom.2018.08.082.

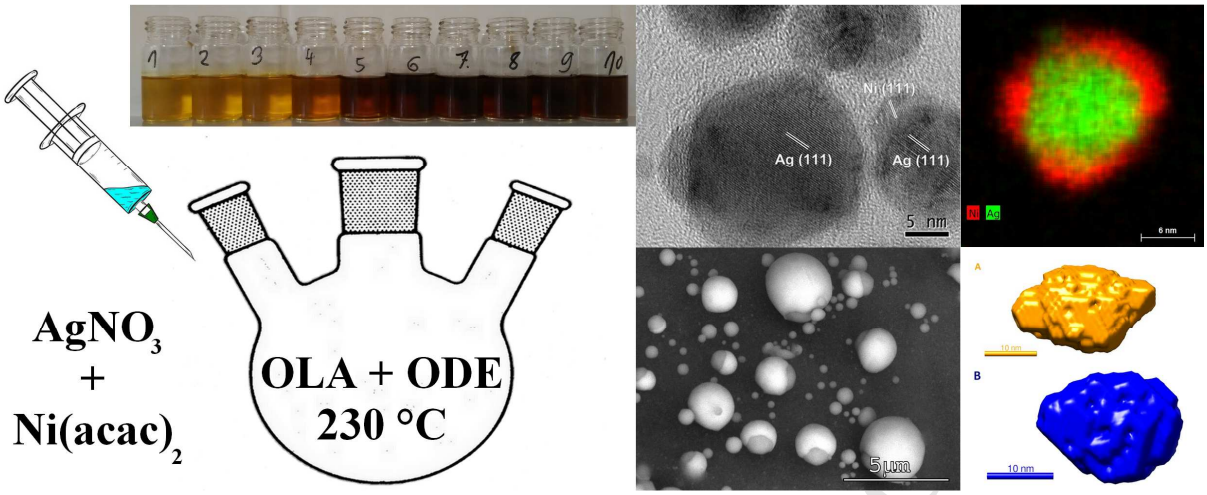

Solvothermal Hot Injection Synthesis of Core-Shell AgNi Nanoparticles

Vit Vykoukal[a,b], Jiri Bursik[c], Pavla Roupcova[c], David A. Cullen[d], Jiri Pinkas[* a,b]

[a] Masaryk University, Faculty of Science, Department of Chemistry, Kotlarska 2, 611 37 Brno, Czech Republic

[b] Masaryk University, CEITEC MU, Kamenice 5, 625 00 Brno, Czech Republic

[c] Institute of Physics of Materials, ASCR, Zizkova 22, 616 62 Brno, Czech Republic

[d] Oak Ridge National Laboratory, 1 Bethel Valley Road, 37830 Oak Ridge, Tennessee, USA

jpinkas@chemi.muni.cz

Abstract

Silver-nickel core-shell nanoparticles (NP) were prepared by solvothermal hot injection synthesis by simultaneous thermolysis/reduction of $AgNO_3$ and $Ni(acac)_2$ precursors in the hot mixture of octadecene and oleylamine. Oleylamine decreases decomposition temperature of $AgNO_3$ to that of $Ni(acac)_2$ thus ensuring favorable reaction conditions. The prepared AgNi NPs with different Ag/Ni ratios were completely characterized. Dynamic light scattering (DLS) and small angle X-ray scattering (SAXS) were used for particle size characterization of as-prepared AgNi colloids. There is no dependence of the particle size (13–21 nm by SAXS) on the Ag/Ni stoichiometric ratio, but the ultraviolet-visible spectroscopy (UV-vis) reveals that the intensity of the surface plasmon (SPR) decreases with increasing Ni content. Transmission electron microscopy (TEM) verified the results of DLS and SAXS and showed spherical nanoparticle shape. Distribution of individual elements in the nanoparticles was mapped by high resolution scanning transmission electron microscopy and energy dispersive X-ray spectroscopy (STEM-EDS) and revealed their core-shell structure where an Ag nucleus is covered by a thin amorphous Ni layer. Upon heating to 400 °C, Ni crystallization is substantiated by appearance of diffractions in the high-temperature X-ray powder diffractograms (HT-XRD) and of a magnetic moment. Ultimate phase separation was proven by scanning electron microscopy and energy dispersive X-ray analysis (SEM-EDS) in samples heated to 1000 °C. The reaction course and nanoparticle formation studied by DLS,

UV-vis, and Ag and Ni elemental analyses reveal an initial Ag seed formation with subsequent Ni overlayer deposition after 180 s.

Keywords

Nanostructured materials; metals and alloys; chemical synthesis; Energy-dispersive X-ray spectroscopy; magnetic measurements; transmission electron microscopy

1. Introduction

Synthesis of metal nanoalloys is nowadays a very attractive and progressive topic, which is intensively studied in academic and industrial laboratories [1]. The preparation of nanoalloys is a challenging task due to their chemical, phase, and morphological variability. High emphasis is especially placed on control of chemical composition, crystal structure, size, and shape and on tunability of their optical, magnetic, thermal, and catalytic properties [2].

Nanoalloys can be prepared by several methods. Among them the solvothermal reduction is highly advantageous, especially if it is carried out in long-chain alkylamines, as they can act as high boiling point solvents, reducing agents, and surface capping species at the same time. This technique produces well-dispersed, monodisperse nanoparticles of metals and metal alloys. For example, silver nanoparticles (NPs) were prepared in dodecylamine at 190–200 °C [3]. Other long-chain alkylamines, such as octylamine, hexadecylamine, and oleylamine, were also used for Ag NPs preparation and their influence on the properties was observed. Different alkylamines, for instance, produced NPs with different diameters [4]. It is evident that the nature of long-chain alkylamines has a high impact on the NP formation. The most commonly used long-chain alkylamine in NP synthesis is oleylamine [5] which is liquid at laboratory temperature unlike saturated alkylamines, which are solid. Oleylamine was used both for single-metal NP preparation, such as Ag [6] and Ni [7–12], and for nanoalloy NPs, such as CuNi [13,14], CuAg [15,16], PdNi [17], AuAg [18], AuPd [19], and PtNiFe [20]. Oleylamine acts as a solvent, an electron donor, and capping agent. The reaction pathway of reduction of a Cu(II) precursor to Cu nanoparticles was studied and oleylamine was shown to be oxidized to imine by beta-H elimination [21]. A different process was observed in reduction of CoO to Co where C–N bond cleavage and beta-H elimination resulted in NH_3 and CO evolution and formation of olefins [22].

The AgNi alloy is a classic example of a system with immiscible components both in liquid and solid state [23]. This large miscibility gap is caused by a large difference in atomic radii (14%) and positive heat of mixing (+15 to +23 kJ mol^{-1}) [24–26]. According to molecular dynamics simulations [27] and density-functional theory (DFT) calculations [28], small AgNi clusters (300−1400 atoms) form almost perfect core-shell structures, where Ni creates the core covered with an Ag shell. The clusters can have either centered or off-center cores. These structures are the most favorable both from the energetic and the kinetic point of view. The Ni@Ag structure of small clusters (2−5 nm) was demonstrated experimentally by low frequency Raman scattering [29] and low-energy ion spectroscopy [30,31].

Ni@Ag core-shell nanoparticles were synthesized by a two-step reduction. First, a Ni^{2+} precursor was reduced by hydrazine to 9.2 nm Ni nanoparticles and then these Ni cores were re-dispersed in an Ag^{+} precursor solution. Added hydrazine completely coated the surface of Ni cores with the Ag shell [32]. The same result was obtained by galvanic coating of Ag on Ni seeds [33]. Nanoparticles with an inverted Ag@Ni core-shell structure have also been synthesized. They were prepared by a facile one-step synthesis in water-in-oil microemulsions [34] or by a one-pot solvothermal synthesis in oleylamine [35]. Several routes to solid-solution AgNi nanoparticles have also been reported. Precursors could be decomposed by ^{60}Co γ source [36,37], reduced by $NaBH_4$ [24,38–40], or hydrazine [41]. In addition, amorphous structures that are nonuniform on an extremely small scale were obtained by vapor quenching of magnetron sputtered alloys [42,43]. Mixing of components and formation of solid solution is favored as the size of particles decreases. Positive enthalpy of mixing has to be overcome by energy input, such as in laser ablation [44–46], laser liquid solid interaction [47,48], magnetron sputtering [47,24], Xe beam mixing [50], or vapor condensation [51,52]. AgNi nanoparticles have been prepared in a solid solution form by reduction of a film containing Ag^{+} and Ni^{2+} ions in a fatty acids matrix by hydrazine vapors [53]. AgNi could be used as a catalyst for the generation of high-purity hydrogen by hydrolysis of $NaBH_4$ [35], hydrogen transfer reaction, hydrogenation of carbonyl compounds [54] or for multiple reduction [55]. Giant magnetoresistance (GMR) was observed in heterogeneous alloy films [56]. AgNi NPs were also studied for electromagnetic radiation shielding applications [25].

Herein we describe the synthesis of AgNi core-shell NPs by the solvothermal hot injection method from $AgNO_3$ and $Ni(acac)_2$ in a mixture of dry oleylamine and 1-octadecene at 230 °C. Nanoparticles with different Ag/Ni compositions are characterized by a variety of microscopic, spectroscopic and analytical techniques revealing their core/shell structure where Ag nucleus is covered by a thin amorphous Ni layer.

2. Experimental section

2.1 Preparation of AgNi NPs

$Ni(acac)_2$ was purchased from Sigma-Aldrich and used as received. $AgNO_3$ was of in-house stock. Oleylamine (with content of 80–90 %) and 1-octadecene (90 %) were purchased from Sigma-Aldrich, dried over sodium, distilled under reduced pressure and stored in a Schlenk flask with molecular sieves.

For a typical synthesis $Ni(acac)_2$ and $AgNO_3$ (at different Ag/Ni ratios, the total amount of 0.4 mmol) were placed in a Schlenk flask and evacuated/refilled with dry N_2 three times. Then dry oleylamine (4 cm^3) was added by a syringe. The mixture was heated to 85 °C to dissolve precursors to a clear green solution. Oleylamine (16 cm^3) and 1-octadecene (20 cm^3) were added into a three-neck Schlenk flask and heated to 120 °C under reduced pressure to remove residual water and oxygen. After 20 min, vacuum was exchanged for dry N_2 and the temperature was increased to 230 °C. The Ag/Ni precursor solution was rapidly injected to the hot mixture of solvents accompanied by a color change to black. After 10 min, the reaction mixture was cooled down to room temperature in a water bath and acetone (20 cm^3) was added to increase the yield by aggregating NPs. The precipitate is then easily separated by centrifugation and redispersed in hexane. The product was washed twice by a mixture of hexane and acetone (1:3 volume ratio) and finally dispersed in hexane and characterized. A yield of 82.5 % was determined by ICP-OES. Pure Ni and Ag NPs were synthesized for the sake of comparison by the same method using a single precursor.

2.2 Reaction course measurements

The oleylamine solution (4 cm^3) of metal precursors (1:1 molar ratio) was injected into a hot mixture (230 °C) of oleylamine and octadecene. Aliquotes (1 cm^3) of this reaction mixture were withdrawn every 30 s and added to 10 cm^3 of cold hexane. These solutions were characterized by the DLS method. For the subsequent UV-vis measurements, the solutions were further diluted by hexane to 1/3 concentration (1 cm^3 of solution + 2 cm^3 of hexane). Finally, acetone (5 cm^3) was added to 5 cm^3 portions of the original solutions, centrifuged, decanted, and the dried precipitates were characterized for Ag and Ni content by ICP-OES.

2.3 Characterization of AgNi NPs

Thermal stability of nanoparticle precursors was studied by the TG-DSC technique on a STA 449C Jupiter (Netzsch) apparatus from 25 to 500 °C under flowing nitrogen (70 cm^3 min^{-1}) with a heating rate of 5 K min^{-1}. The $Ni(acac)_2$ and $AgNO_3$ precursors (~15 mg) were

placed into alumina crucibles and heated first without and then with a large excess of oleylamine (0.05 cm^3)

The hydrodynamic diameter was determined by the dynamic light scattering (DLS) technique on a Zetasizer Nano ZS (Malvern) instrument in hexane solution at 25 °C. The samples were diluted and filtered by a syringe filter (pore size 450 nm) to remove aggregates and impurities. When the results were polydisperse, sedimentation was used for removing of distorting influences. Each DLS result is an average of three measurements.

Small angle X-Ray scattering (SAXS) measurements were carried out on a Biosaxs 1000 (Rigaku) system at 25 °C with λ = 14 nm for 5 min. The samples were sealed in 1.5 mm (O.D.) borosilicate glass capillaries (WJM-Glas). Data were analyzed by both Primus and Gnom software and the results were mutually compared.

The UV-vis spectra were obtained on a Unican UV4 (Chromspec) spectrometer. The samples were prepared by the same procedure as for DLS, but they were diluted to one fourth.

The AgNi NPs were characterized by transmission and scanning electron microscopy (TEM, SEM). The TEM measurements were carried out on a CM 12 TEM/STEM (Philips) microscope with EDAX Phoenix EDS and on a JEOL JEM2010F microscope equipped with an EDS detector and a CCD camera with resolution of 1024x1024 pixels. The samples for the TEM measurements were dispersed in hexane and one drop of the colloidal solution was placed on a carbon-coated copper grid and allowed to dry by evaporation at ambient temperature. STEM-EDS spectrum imaging of single nanoparticles was performed on an FEI Talos F200X S/TEM microscope equipped with a ChemiSTEM Super-X EDS system. For the SEM analysis, the samples were dried at ambient temperature under inert atmosphere. Analyses were performed on a LYRA 3 XMU FEG/SEM-SIB microscope (Tescan) with an Oxford Instruments X-Max80 analyzer for EDS analysis.

Powder X-ray diffraction (PXRD) measurements were carried out on a SmartLab (Rigaku) diffractometer with a linear detector, with a Cu lamp, fine focus $\lambda_{K\alpha1}$ = 15.4060 nm, $\lambda_{K\alpha2}$ = 15.4443 nm and $\lambda_{K\beta}$ = 13.9225 nm. The samples were measured in a parallel beam order in a transmission mode between two foils. High temperature measurements (HT XRD) were carried out with samples placed in an HTK-16N Anton Paar heating chamber with a platinum strip under He atmosphere. The heating rate was 5 K min^{-1}, delay 40 s and measurement time 2 min at every temperature. The HT-XRD pattern computation enabled the identification of the coexisting phases and evaluation of their lattice constants and average coherent domain sizes (crystallinity) using the Rietveld-assisted Debye Scherrer equation.

Vibrating sample magnetometry was measured on an EG&G Applied Research Corporation Model 4500 instrument. Dry powders were compressed to pellets. The samples were also heated with a heating rate of 4 K min^{-1}.

The metal content was analyzed by inductively coupled plasma optical emission spectroscopy (ICP-OES) on an iCAP 6500 Duo (Thermo) spectrometer. The dried AgNi NPs were completely dissolved in HNO_3, diluted, and characterized. Elemental analyses (C, H, and N) were performed on an EA-1108 Analyzer (Fisons Instruments) at UP Olomouc.

3. Results and discussion

$AgNO_3$ and $Ni(acac)_2$ are common precursors for the synthesis of corresponding metal and metal oxide nanoparticles [3,6–8,10–12,24,34,35,38–41,54]. We used thermal analysis to compare their stability and decomposition behavior under N_2 in order to use them for the hot-injection synthesis of the AgNi alloy NPs. Silver nitrate is a relatively stable chemical compound (mp 212 °C, bp 440 °C dec.). In our TG/DSC experiment (Fig. S1†), it decomposed at 460 °C under nitrogen. The total mass loss of 36.5 % is in accordance with the expected value for its conversion to metallic Ag (36.50 %). Two endothermic effects at 162 °C and 209 °C were assigned to the modification changes and melting point, respectively [57]. In the presence of excess oleylamine (bp ~364 °C), $AgNO_3$ is thermally decomposed already at 212 °C (Fig. S1†). The TG/DSC analysis of $Ni(acac)_2$ showed an endothermic effect at 225 °C which is close to its melting point (229 °C) (Fig. S2†). This temperature is also the onset of multistep $Ni(acac)_2$ decomposition [58]. The observed total mass loss of 78.0 % is in agreement with the theoretical value for the conversion to metallic Ni (77.16 %). Thermal behavior of $Ni(acac)_2$ in excess oleylamine was completely different as it abruptly transformed at 225 °C to metallic Ni (Fig. S3†). Both precursors thus decompose in oleylamine at similar temperatures and could be used for the AgNi NP preparation by the solvothermal hot injection synthesis at 230 °C. 1-octadecene was added as a co-solvent based on related synthetic procedure [13]. The reactions were carried out by a standardized protocol with the Ag/Ni stoichiometric ratios given in Table 1. The nominal Ag/Ni ratios of the precursor mixtures are reflected in the elemental composition of the isolated nanoparticles (ICP-OES) attesting to complete decomposition of both precursors.

The dependence of nanoparticle size on their elemental composition (ICP-OES) was studied by the DLS technique which provides three types of data for description of prepared

nanoparticles. The particle sizes expressed as Z-averages are summarized in Table 1 and the weighted averages of hydrodynamic diameter (based on light intensity) and polydispersity indices (PdI) are given in Table S1†. The Z-average values can be used for comparison with sizes obtained by other characterization techniques, such as SAXS. This comparison is given in Table 1. Models of average AgNi nanoparticles have been calculated based on the SAXS data by ab initio calculation (Fig. S4†). They show an irregular particle for a high Ni content while a nearly spherical shape resulted for a low Ni content [59].

The AgNi NPs phase composition and particle size have been characterized by the PXRD technique and by application of the Rietveld-assisted Debye-Scherrer equation. The as-prepared nanoparticles were dried under flow of dry nitrogen and then measured. The PXRD measurements of these nanopowders revealed only the fcc Ag diffractions. This effect could be explained in combination with the TEM/STEM/EDS and HRTEM results (see below). Nickel creates a thin layer on the silver core and behaves as amorphous or poorly crystalline material and thus could not be detected by PXRD. Nickel crystallization with increasing temperature is confirmed by appearance of its diffractions during the HT-XRD measurement at 400 °C (see below). Average coherent domain sizes and lattice parameters (*a*) of the as-prepared AgNi NPs were calculated. There is no dependence of diameter on the composition. Also the lattice constant displays non-Vegard behavior because of immiscible nature of the AgNi system and metal separation in core/shell NPs.

Table 1: DLS, SAXS and PXRD characterization of particle size for the AgNi NPs with different compositions

Ag (mol%) Nominal	10	20	31	39	41	54	60	59	70	75	80
Ag (mol%) ICP-OES	11	18	32	41	49	59	60	63	73	77	83
DLS[a] (*d* = nm)	28	28	25	26	23	28	28	25	25	31	25
SAXS (*d* = nm)	-	-	15.2	14.9	12.8	20.5	-	14.9	18.2	-	20.9
PXRD[b] (*d* = nm)	-	11.1	6.7	-	6.6	7.9	-	-	6.9	-	6.7
a (Å)	-	4.089	4.093	-	4.094	4.091	-	-	4.104	-	4.094

[a] Z-Average. [b]Average coherent domain size.

As can be gleaned from Table 1, the Ag/Ni ratio has only an insignificant effect on the particle size obtained by all three methods. The samples were in fact monodisperse or only slightly polydisperse according to the DLS and SAXS measurements. The SAXS method is sensitive to differences in electron density (12.8–20.9 nm) while DLS measures larger hydrodynamic diameter (23–31 nm) which includes the surface organic layer. The SAXS data were analyzed by both Primus and Gnom programs. Primus can fit and evaluate the integral parameters from Gunnier and Porod plots, such as the radius of gyration. Gnom can evaluate the particle distance distribution function (monodispersive function) and the size distribution function (polydispersive function) [60]. Both programs were used and the results were mutually compared with the help of special scripts that we wrote for finding the best fit. The results of Primus and Gnom fitting for the AgNi nanoparticles with 73 mol% Ag are compared in Fig. S5 and S6†. Curve fitting is of high quality and fitted data are in full accordance with experimental data in both cases. The most frequent size of the prepared AgNi NPs and radius of gyration are also in excellent agreement. Table 1 summarizes the particle size data obtained from Gnom.

The size, shape, and polydispersity of the AgNi NPs with different compositions were also characterized by TEM (Fig. 1). Pure Ni and Ag NPs were recorded for the sake of comparison (Fig. S7 and S8†). The micrographs of AgNi NPs were analyzed by the ImageJ program and histograms of nanoparticle diameters were obtained. Weighted averages of AgNi NP diameters obtained from TEM are smaller than the ones from DLS and SAXS, because only the metal core of nanoparticles is observed [61]. With increasing silver content the particle size distribution broadens, probably because the nickel layer becomes less compact and regular and forms islands. The calculated nanoparticle models based on the SAXS data (Fig. S4†) are supported by the HRTEM images showing the AgNi NPs as nearly regular cores with several satellites (see below).

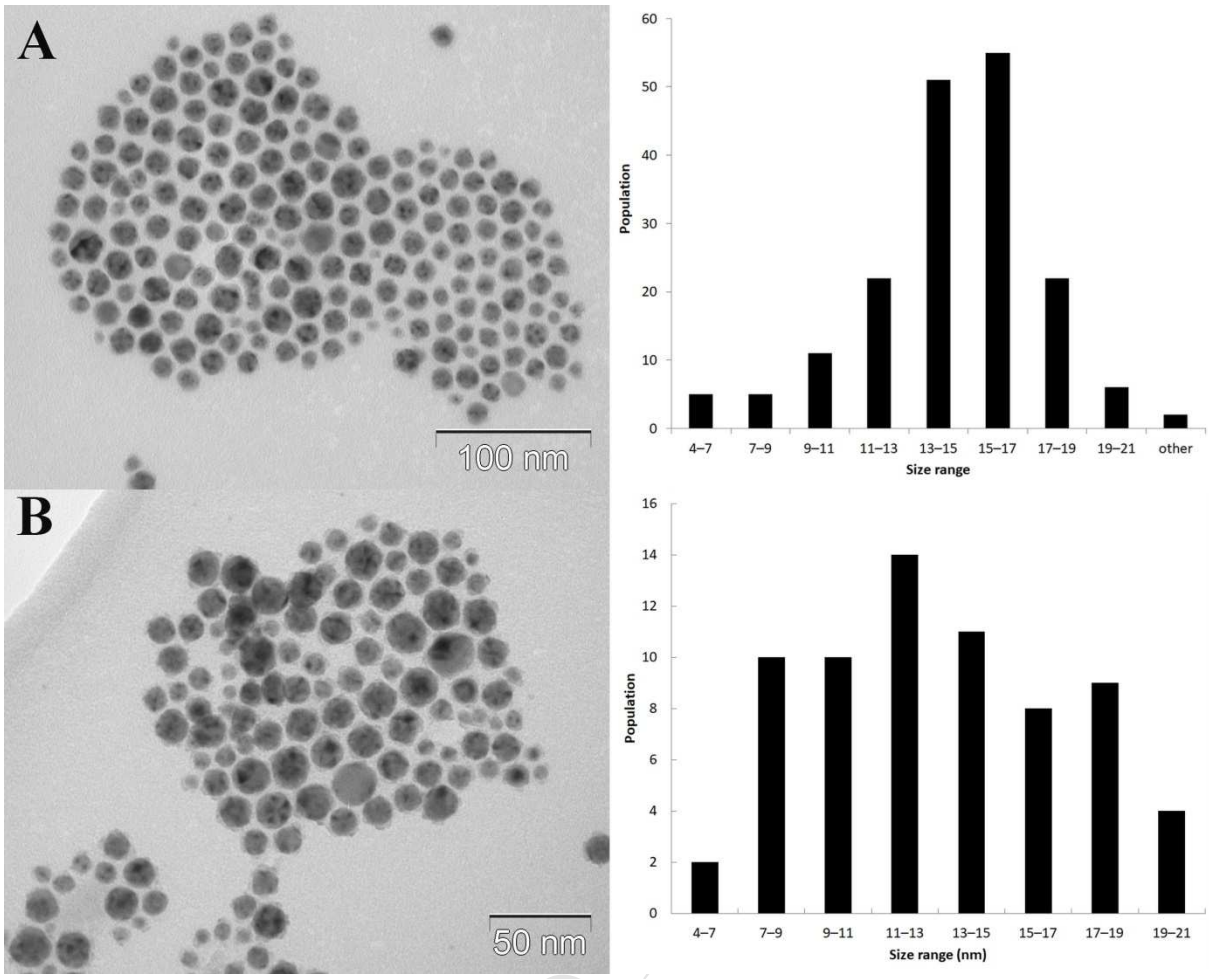

Fig. 1. TEM image of AgNi NPs Ag 59 mol% $\bar{x}$ = 15 nm (A) and 83 mol% $\bar{x}$ = 14 nm (B)

The spatial distribution of Ag and Ni elements in individual nanoparticles was characterized by the high-resolution STEM-EDS. Fig. 2 shows core/shell structures of the AgNi NPs. The silver nucleus is covered by a thin, nonuniform layer of nickel. The nickel shell does not completely cover the silver core in nanoparticles with a low Ni content. In both examined samples, STEM-EDS quantification of the particle compositions showed a significantly higher Ag content, suggesting that not all the Ni present in the sample had deposited on the Ag cores.

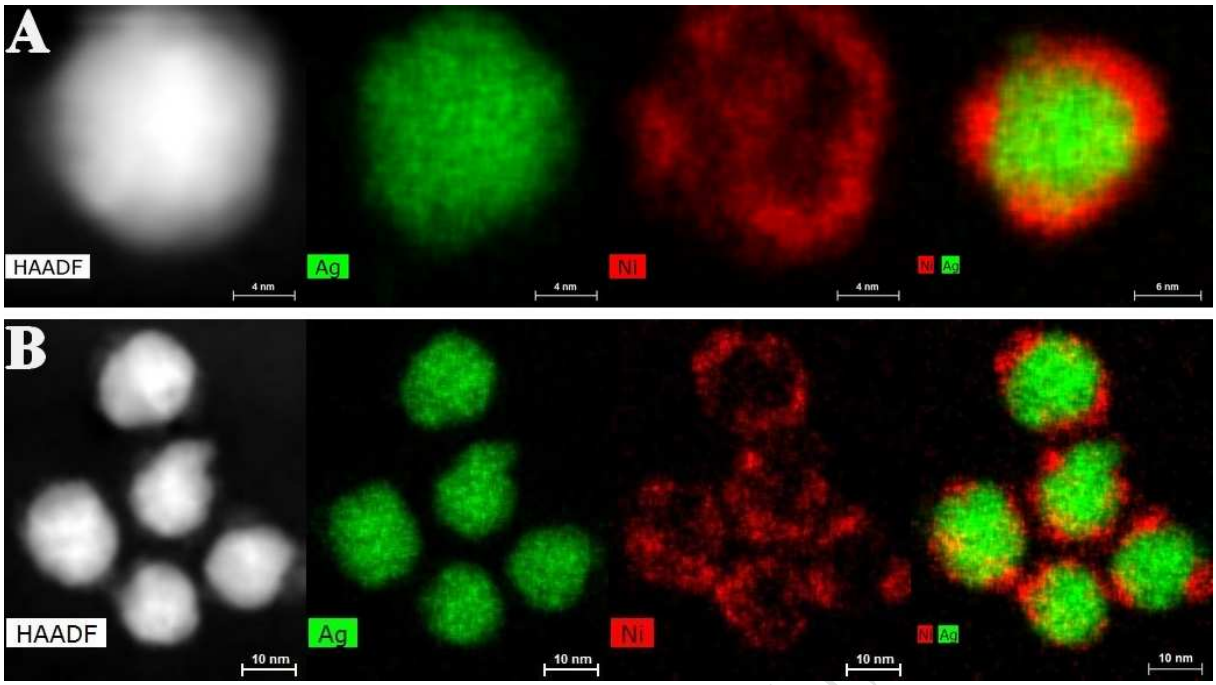

Fig. 2. STEM-EDS analysis of AgNi NPs ICP-OES: Ag 50.3 mol%, EDS: Ag 62.5 mol% (A) and ICP-OES: Ag 68.8 mol%, EDS: Ag 84.2 mol% (B)

HRTEM micrographs of nanoparticles in Fig. 3 display the frequent case when darker nearly spherical particles have several satellites of presumably lower density (marked by arrows). In several cases the lattice fringes were observed in the satellites. Quantitative evaluation of interatomic distances supports the scenario observed in high resolution EDS maps (Fig. 2); i.e. Ag cores are covered by several discontinuous outer regions of Ni.

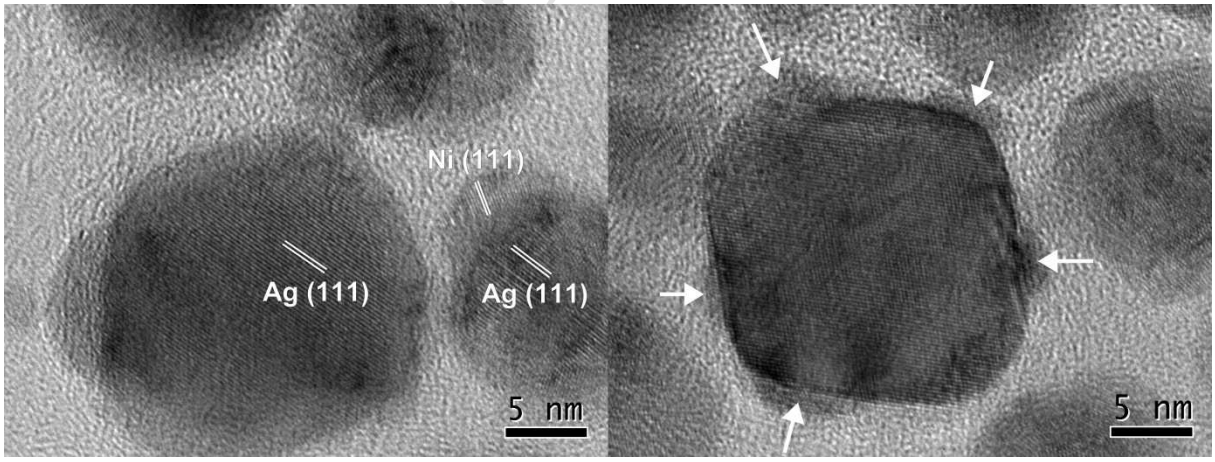

Fig. 3. HRTEM analysis of AgNi NPs (ICP-OES: Ag 58.8 mol%)

The prepared colloidal solutions of AgNi NPs with different Ag/Ni ratios were examined by the UV-vis spectroscopy. The spectra of Ag and Ni metal NPs and of free oleylamine are shown for comparison in Fig. S9†. Surface plasmon resonances (SPR) of AgNi NPs with different Ag/Ni compositions were observed in range of 347–404 nm (Fig. 4), but this shift is

not caused by composition change but rather by reduction of the Ag core size. This is in contrast to the SPR of the AgAu nanoparticles, whose wavelength depends on the nanoalloy composition and is red shifted with increasing Au content [62]. In small clusters of AgNi (2–5 nm) which form core-shell structures, where Ag covers the Ni nucleus, a blue shift of the resonance band as well as damping and broadening with increasing Ni proportion was observed [30]. On the contrary, AgNi nanoparticles with a bigger diameter than 6 nm are reported to feature decreasing SPR absorption intensity and broadening peak widths with increasing Ni concentration [41]. In the case of AgNi, the phenomenon of plasmon maximum shift was observed and it is probably caused by smaller diameter of silver nuclei. The dependence of absorbance intensity on the AgNi NPs composition was observed.

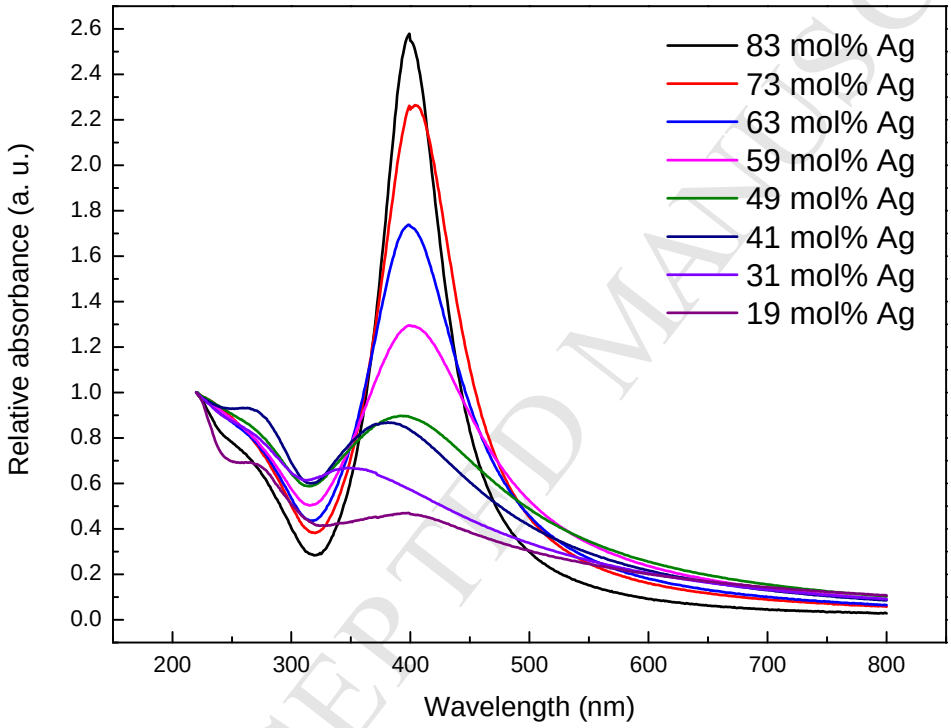

Fig. 4. SPR of AgNi NPs with different compositions

The AgNi nanopowders were also studied by HT-XRD during and after annealing. A spontaneous decomposition of coherent AgNi to a silver-rich phase and a nickel-rich phase was observed Fig. 5. At the same time an increase of the average coherent domain size and lattice parameters for both phases were also evident. The AgNi samples were placed onto a platinum holder and heated from the reference temperature of 30 °C to 650 °C with a heating ramp of 5 K min^{-1}. The X-ray diffractograms were collected in 10 °C steps up to the final temperature. A phase separation was observed at 400–410 °C for the 41 mol% Ag nanoparticles (Fig. S10†). In case of a higher concentration of Ag, the phase separation was

detected in two steps, the first at 370–380 °C and the second at 400–430 °C for the 60 mol% Ag NPs (Fig. S11†). In these intervals we observed by the Rietveld analysis an increasing amount of the crystalline Ni-rich phase, whose content was practically constant above this point.

For the 41 mol% Ag NPs, the average coherent domain size of the Ag-rich phase was practically linearly growing from 6.2 nm at 320 °C to the maximum of 61.8 nm at 640 °C (Fig. S12†). The Ni-rich phase was first observed at 410 °C and its size was growing from 7 to 50 nm at the final temperature of 650 °C. For the NPs with a higher Ag concentration (60 mol% Ag), the growth of the average coherent domain size was slightly different (Fig. S14†). The trend of growing size from around 300 °C is the same for the Ag-rich phase as in the previous case. The average coherent domain size is constant from 100 to 300 °C and a rapid growth begins at 350 °C (10.2 nm) and at 600 °C reaches 100.4 nm (Fig. S14†). The Ni-rich phase appeared at 430 °C (7.2 nm) and it was growing during heating to the final size of 35.1 nm at 600 °C.

The lattice parameter increase was also detected in both phases during heating. For the 41 mol% Ag NPs, the Ag-rich phase displayed the lattice parameter of 4.075 Å at 100 °C and it was constantly growing to 4.134 Å at 650 °C (Fig. S13†). The Ni-rich phase was at first rapidly growing from 3.531 Å at 410 °C to 3.548 Å at 450 °C and then slowly growing to 3.554 Å at 650 °C. For the 60 mol% Ag NPs, the lattice parameter of the Ag-rich phase was 4.090 Å at 100 °C and it grew in two steps. The first step was detected at 269 °C (4.100 Å) and the second at 360 °C (4.109 Å) (Fig. S15†). From this point the lattice parameter was constantly growing to the final value of 4.134 Å at 650 °C. The Ni-rich phase showed a constant parameter from 360 °C to 410 °C (3.502 Å) and then rapid growth to 3.553 Å at 450 °C. From 450 °C to 650 °C the lattice parameter was practically constant (at 650 °C 3.558 Å) (Fig. S15†). The lattice parameters have shown a good agreement when compared with literature data [63].

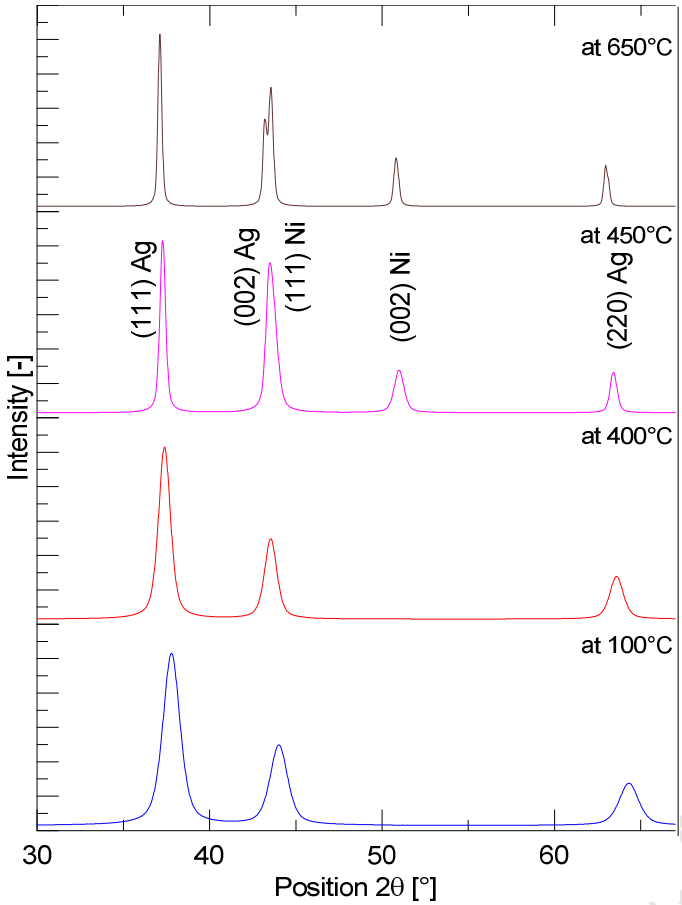

Fig. 5. HT-XRD of AgNi NPs with 40 mol% Ag

The phase separation in the AgNi samples heated to 1000 °C was confirmed by the SEM-EDS measurements (Fig. 6 and Fig. 7). Darker areas in the SEM micrographs with backscattered electrons were characterized as the Ni-rich phase and lighter ones as the Ag-rich phase, and their phase separation is evident. The Ni-rich phase is embedded in the Ag-rich matrix. The most significant manifestation of the phase separation is the formation of Janus particles which are clearly displayed in Fig. 7 where the particles formed after annealing to 1000 °C were characterized by elemental mapping.

Spectrum	Ni (mol%)	Ag (mol%)
1	97.58	2.42
2	97.33	2.67
3	6.93	93.07
4	6.54	93.46

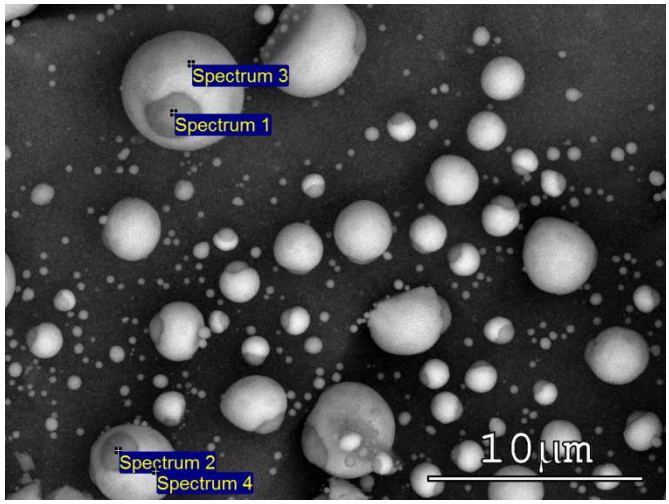

Fig. 6. SEM-EDS analysis of AgNi nanoparticles (59 mol% Ag) after annealing to 1000 °C

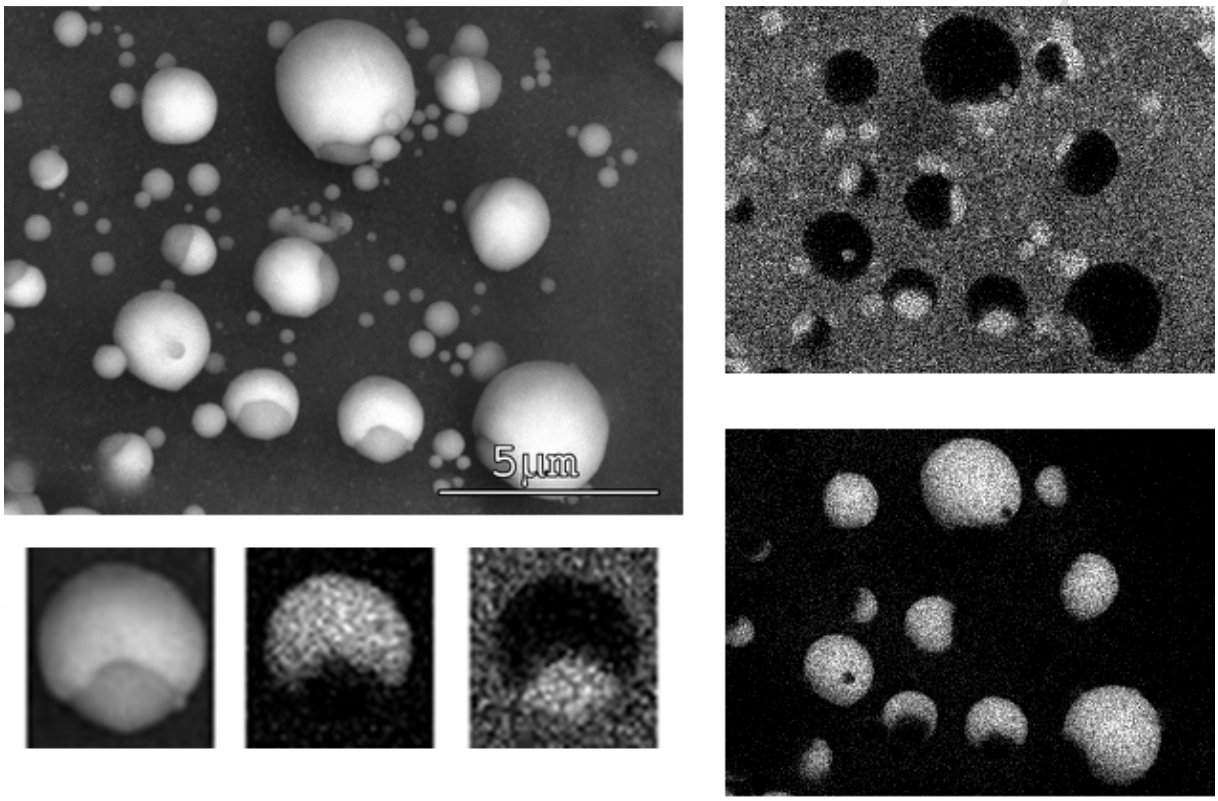

Fig. 7. SEM-EDS spectrum images of AgNi nanoparticles (59 mol% Ag) after annealing to 1000 °C

The characterization of magnetic properties of the AgNi NPs provides additional information about the prepared nanomaterials. The as-prepared AgNi NPs do not display any magnetic properties. It confirms the results from TEM/STEM/EDS and HRTEM that nickel is almost amorphous, there is not enough crystalline material for detection of any magnetic properties. Magnetic moments of the AgNi NPs (with different amounts of Ni) were measured before and after annealing to 450 °C when the phase separation occurred. The AgNi NPs do not feature any magnetic moment before crystallization of nickel. When magnetic moments of annealed nanoparticles are compared, it is evident that the AgNi NPs with a higher concentration of Ni exert a higher magnetic moment (Fig. 8). Onset temperatures of magnetic moment appearance were also studied. In case of the 23.4 mol% Ni nanoparticles, magnetic moment was observed at 351 °C and in case of the 75.6 mol% Ni NPs it appeared at 356 °C.

This effect occurred exclusively during cooling down. The magnetic moments were not evident during heating (Fig. S16†).

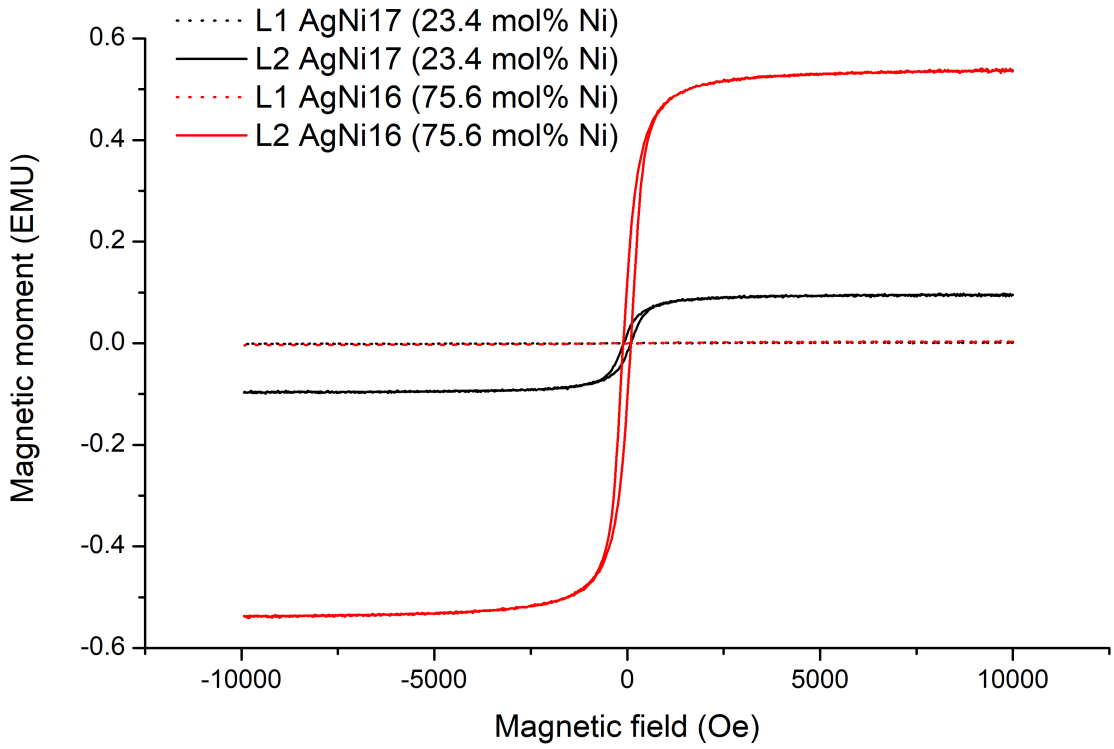

Fig. 8. VSM of AgNi nanoparticles with different compositions before (L1) and after (L2) annealing to 450 °C

The course of the AgNi formation during the thermolysis reaction was studied by following the particle size, the SPR maximum, and the chemical composition as a function of time. The reaction was conducted in a manner described in the Experimental section. The AgNi nanoparticle precipitates were isolated and purified. The results are summarized in Fig. 9 and in Table S2 and show the presence of NPs already after the first 30 s. The UV-vis spectra looked very similar with three maxima. The first two at 220 nm and 300 nm belong to oleylamine on the surface of the AgNi NPs and the third peak at 400 nm belongs to the silver SPR. The intensity values for Ag SPR are shown in Table S2 relative to the intensity of oleylamine peak at 220 nm which is considered to remain constant. The DLS results show that nanoparticles appeared practically immediately after the injection of the precursor solution and they were growing from 20 to 30 nm with time. The first step of diameter growth was determined after 180 s. The intensity of the silver SPR was slightly decreasing for the first six samples, after 180 s the intensity of the silver SPR abruptly decreased. The elemental analysis showed that nanoparticles formed after the precursor injection contained practically

only silver. Nickel started to be slowly reduced at 180 s and rapidly at 210 s. When the results are mutually compared it is evident that the most interesting step of the AgNi NP synthesis is around 180 s of the reaction time when the composition of nanoparticles changed to the final ratio, the UV-vis spectra show a rapid decrease of the Ag SPR intensity, and the DLS results show growth of nanoparticles.

Monitoring the progress of the reaction confirms the formation of core-shell structures. DLS shows nanoparticles arising in the first 30 seconds. Optical properties and elemental analysis demonstrate that the reaction proceeds in two steps. In the first stage, the Ag precursor is reduced and forms the nuclei and the relative absorbance of Ag SPR is the highest. Subsequently nickel is reduced and deposited as a shell on the silver cores, causing decreasing of the Ag SPR intensity. This conclusion is consistent with elemental distribution in the as-prepared AgNi NPs characterized by TEM/STEM-EDS.

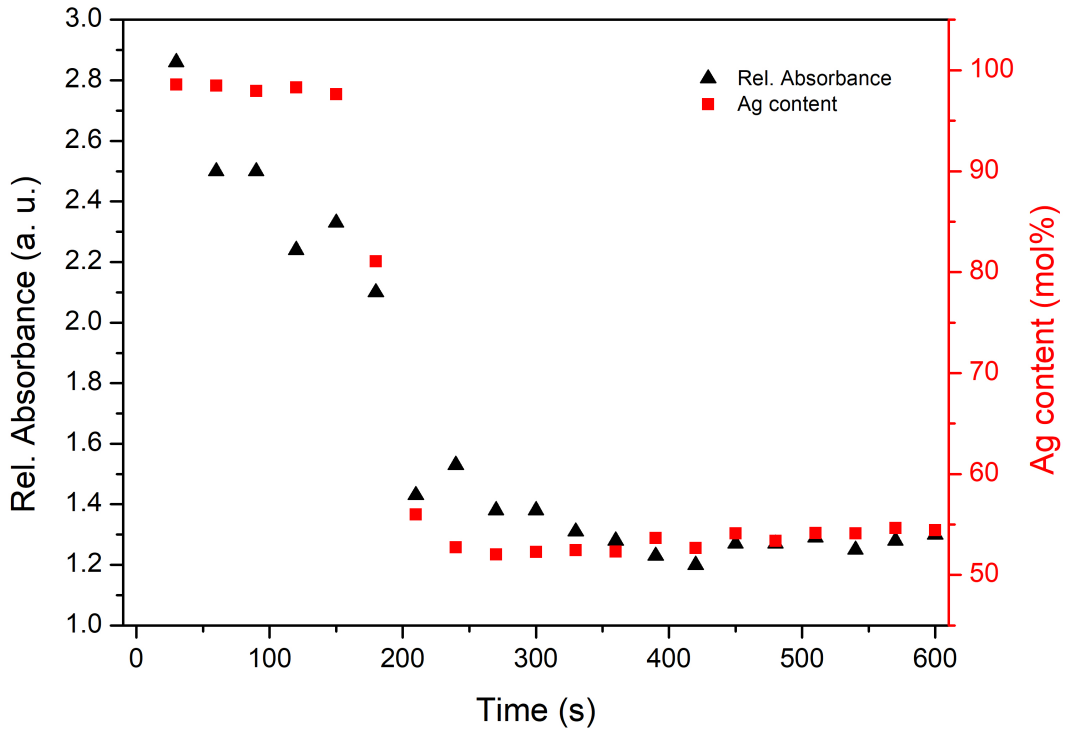

Fig. 9. SPR absorbance at 400 nm and Ag content of AgNi NPs as a function of time

4. Conclusions

AgNi nanoparticles were prepared by solvothermal hot injection synthesis with different Ag/Ni stoichiometric compositions. This method extends available synthetic routes to the

nanoalloy systems. Oleylamine served as solvent and more importantly it also equalized decomposition temperatures of metal precursors. However following the time evolution of the thermolysis reaction, the initial formation of Ag nuclei was observed within the first 3 min with subsequent Ni deposition leading to the core-shell structure which is inverted with respect to theoretical predictions. Nanoparticles featuring crystalline silver cores and amorphous nickel shells were characterized by variety physical/chemical techniques. Dependence of particle size on chemical composition was not observed. The SPR absorption was studied as a function of the Ag/Ni ratio and it was found that with increasing concentration of Ni the SPR intensity was decreasing. Ni crystallization was demonstrated during heating to 400 °C and complete phase separation to Janus type particles occurred at 1000 °C. These effects were proven by several methods, such as SEM-EDS, VSM, and HT-XRD. The prepared AgNi core-shell nanoparticles will be tested as potential catalysts in hydrogenation reactions.

Conflicts of interest

There are no conflicts of interest to declare.

Acknowledgement

The results of this research have been acquired within the CEITEC 2020 (LQ1601) project with financial contribution made by the MEYS CR within special support paid from the National Program for Sustainability II funds and by the Czech Science Foundation (GA 17-15405S). CIISB research infrastructure project LM2015043 funded by MEYS CR is gratefully acknowledged for the financial support of the measurements at the CF X-ray Diffraction and Bio-SAXS. The authors thank Dr. K. Novotny and L. Simonikova for ICP-OES analyses, Dr. O. Schneeweiss for magnetic and Dr. Z. Moravec for TG-DSC measurements. STEM-EDS analysis was performed as part of a user project through Oak Ridge National Laboratory's Center for Nanophase Materials Sciences, which is a U.S. Department of Energy (DOE) Office of Science user facility along with instrumentation provided by the DOE Office of Nuclear Energy, Fuel Cycle R&D Program, and the Nuclear Science User Facilities.

Appendix A. Supplementary data

Supplementary data related to this article can be found at https://doi.org/XXXX

References

[1] R. Ferrando, J. Jellinek, R.L. Johnston, Nanoalloys: From Theory to Applications of Alloy Clusters and Nanoparticles, Chem. Rev. 108 (2008) 845–910. doi:10.1021/cr040090g.

[2] K.D. Gilroy, A. Ruditskiy, H.-C. Peng, D. Qin, Y. Xia, Bimetallic Nanocrystals: Syntheses, Properties, and Applications, Chem. Rev. 116 (2016) 10414–10472. doi:10.1021/acs.chemrev.6b00211.

[3] D. Wakuda, K.-S. Kim, K. Suganuma, Room temperature sintering of Ag nanoparticles by drying solvent, Scr. Mater. 59 (2008) 649–652. doi:10.1016/j.scriptamat.2008.05.028.

[4] Y. Kashiwagi, M. Yamamoto, M. Nakamoto, Facile size-regulated synthesis of silver nanoparticles by controlled thermolysis of silver alkylcarboxylates in the presence of alkylamines with different chain lengths, J. Colloid Interface Sci. 300 (2006) 169–175. doi:10.1016/j.jcis.2006.03.041.

[5] S. Mourdikoudis, L.M. Liz-Marzán, Oleylamine in Nanoparticle Synthesis, Chem. Mater. 25 (2013) 1465–1476. doi:10.1021/cm4000476.

[6] M. Chen, Y.-G. Feng, X. Wang, T.-C. Li, J.-Y. Zhang, D.-J. Qian, Silver Nanoparticles Capped by Oleylamine: Formation, Growth, and Self-Organization, Langmuir. 23 (2007) 5296–5304. doi:10.1021/la700553d.

[7] M. Li, Y. Chen, N. Ji, D. Zeng, D.-L. Peng, Preparation of monodisperse Ni nanoparticles and their assembly into 3D nanoparticle superlattices, Mater. Chem. Phys. 147 (2014) 604–610. doi:10.1016/j.matchemphys.2014.05.036.

[8] Y. Pan, R. Jia, J. Zhao, J. Liang, Y. Liu, C. Liu, Size-controlled synthesis of monodisperse nickel nanoparticles and investigation of their magnetic and catalytic properties, Appl. Surf. Sci. 316 (2014) 276–285. doi:10.1016/j.apsusc.2014.07.203.

[9] S. Mourdikoudis, K. Simeonidis, A. Vilalta-Clemente, F. Tuna, I. Tsiaoussis, M. Angelakeris, C. Dendrinou-Samara, O. Kalogirou, Controlling the crystal structure of Ni nanoparticles by the use of alkylamines, J. Magn. Magn. Mater. 321 (2009) 2723–2728. doi:10.1016/j.jmmm.2009.03.076.

[10] J. Park, E. Kang, S.U. Son, H.M. Park, M.K. Lee, J. Kim, K.W. Kim, H.-J. Noh, J.-H. Park, C.J. Bae, J.-G. Park, T. Hyeon, Monodisperse Nanoparticles of Ni and NiO: Synthesis, Characterization, Self-Assembled Superlattices, and Catalytic Applications in the Suzuki Coupling Reaction, Adv. Mater. 17 (2005) 429–434. doi:10.1002/adma.200400611.

[11] S. Carenco, C. Boissière, L. Nicole, C. Sanchez, P. Le Floch, N. Mézailles, Controlled Design of Size-Tunable Monodisperse Nickel Nanoparticles, Chem. Mater. 22 (2010) 1340–1349. doi:10.1021/cm902007g.

[12] K.P. Donegan, J.F. Godsell, D.J. Otway, M.A. Morris, S. Roy, J.D. Holmes, Size-tuneable synthesis of nickel nanoparticles, J. Nanoparticle Res. 14 (2012) 670. doi:10.1007/s11051-011-0670-y.

[13] Y. Zhang, W. Huang, S.E. Habas, J.N. Kuhn, M.E. Grass, Y. Yamada, P. Yang, G.A. Somorjai, Near-Monodisperse Ni−Cu Bimetallic Nanocrystals of Variable Composition: Controlled Synthesis and Catalytic Activity for H_2 Generation, J. Phys. Chem. C. 112 (2008) 12092–12095. doi:10.1021/jp805788x.

[14] J. Sopousek, J. Vrestal, J. Pinkas, P. Broz, J. Bursik, A. Styskalik, D. Skoda, O. Zobac, J. Lee, Cu–Ni nanoalloy phase diagram – Prediction and experiment, Calphad. 45 (2014) 33–39. doi:10.1016/j.calphad.2013.11.004.

[15] J. Sopousek, J. Pinkas, P. Broz, J. Bursik, V. Vykoukal, D. Skoda, A. Styskalik, O. Zobac, J. Vrestal, A. Hrdlicka, J. Simbera, Ag-Cu Colloid Synthesis: Bimetallic Nanoparticle Characterisation and Thermal Treatment, J. Nanomater. 2014 (2014) 1–13. doi:10.1155/2014/638964.

[16] J. Sopousek, O. Zobac, J. Bursik, P. Roupcova, V. Vykoukal, P. Broz, J. Pinkas, J. Vrestal, Heat-induced spinodal decomposition of Ag–Cu nanoparticles, Phys Chem Chem Phys. 17 (2015) 28277–28285. doi:10.1039/C5CP00198F.

[17] S.U. Son, Y. Jang, J. Park, H. Bin Na, H.M. Park, H.J. Yun, J. Lee, T. Hyeon, Designed Synthesis of Atom-Economical Pd/Ni Bimetallic Nanoparticle-Based Catalysts for Sonogashira Coupling Reactions, J. Am. Chem. Soc. 126 (2004) 5026–5027. doi:10.1021/ja039757r.

[18] C. Wang, H. Yin, R. Chan, S. Peng, S. Dai, S. Sun, One-Pot Synthesis of Oleylamine Coated AuAg Alloy NPs and Their Catalysis for CO Oxidation, Chem. Mater. 21 (2009) 433–435. doi:10.1021/cm802753j.

[19] F. Fu, S. He, S. Yang, C. Wang, X. Zhang, P. Li, H. Sheng, M. Zhu, Monodispersed {AuPd} nanoalloy: composition control synthesis and catalytic properties in the oxidative dehydrogenative coupling of aniline, Sci China Chem. 58 (2015) 1532–1536. doi:10.1007/s11426-015-5358-1.

[20] J. Luo, L. Wang, D. Mott, P.N. Njoki, N. Kariuki, C.-J. Zhong, T. He, Ternary alloy nanoparticles with controllable sizes and composition and electrocatalytic activity, J. Mater. Chem. 16 (2006) 1665. doi:10.1039/b518287e.

[21] B. Hou, D. Benito-Alifonso, N. Kattan, D. Cherns, M.C. Galan, D.J. Fermín, Initial Stages in the Formation of $Cu_2ZnSn(S,Se)_4$ Nanoparticles, Chem. - Eur. J. 19 (2013) 15847–15851. doi:10.1002/chem.201302722.

[22] K.M. Nam, J.H. Shim, H. Ki, S.-I. Choi, G. Lee, J.K. Jang, Y. Jo, M.-H. Jung, H. Song, J.T. Park, Single-Crystalline Hollow Face-Centered-Cubic Cobalt Nanoparticles from Solid Face-Centered-Cubic Cobalt Oxide Nanoparticles, Angew. Chem. Int. Ed. 47 (2008) 9504–9508. doi:10.1002/anie.200803048.

[23] M. Singleton, P. Nash, The Ag−Ni (Silver-Nickel) system, J. Phase Equilibria. 8 (1987) 119–121. doi:10.1007/BF02873194.

[24] C. Srivastava, S. Chithra, K.D. Malviya, S.K. Sinha, K. Chattopadhyay, Size dependent microstructure for Ag–Ni nanoparticles, Acta Mater. 59 (2011) 6501–6509. doi:10.1016/j.actamat.2011.07.022.

[25] E. Ma, Alloys created between immiscible elements, Prog. Mater. Sci. 50 (2005) 413–509. doi:10.1016/j.pmatsci.2004.07.001.

[26] O. Proux, J. Mimault, J.R. Regnard, C. Revenant-Brizard, B. Mevel, B. Dieny, Structural coherence between phases in Ni0.35Ag0.65 thin films, J. Phys.-Condens. Matter. 12 (2000) 3939–3953. doi:10.1088/0953-8984/12/17/302.

[27] F. Baletto, C. Mottet, A. Rapallo, G. Rossi, R. Ferrando, Growth and energetic stability of AgNi core-shell clusters, Surf. Sci. 566 (2004) 192–196. doi:10.1016/j.susc.2004.05.044.

[28] K. Laasonen, E. Panizon, D. Bochicchio, R. Ferrando, Competition between Icosahedral Motifs in AgCu, AgNi, and AgCo Nanoalloys: A Combined Atomistic–DFT Study, J. Phys. Chem. C. 117 (2013) 26405–26413. doi:10.1021/jp410379u.

[29] H. Portales, L. Saviot, E. Duval, M. Gaudry, E. Cottancin, M. Pellarin, J. Lerme, M. Broyer, Resonant Raman scattering by quadrupolar vibrations of Ni-Ag core-shell nanoparticles, Phys. Rev. B. 65 (2002) 165422–165426. doi:10.1103/PhysRevB.65.165422.

[30] M. Gaudry, E. Cottancin, M. Pellarin, J. Lerme, L. Arnaud, J.R. Huntzinger, J.L. Vialle, M. Broyer, J.L. Rousset, M. Treilleux, P. Melinon, Size and composition dependence in

the optical properties of mixed (transition metal/noble metal) embedded clusters, Phys Rev B. 67 (2003) 155409. doi:10.1103/PhysRevB.67.155409.

[31] E. Cottancin, M. Gaudry, M. Pellarin, J. Lerme, L. Arnaud, J.R. Huntzinger, J.L. Vialle, M. Treilleux, P. Melinon, J.-L. Rousset, M. Broyer, Optical properties of mixed clusters: comparative study of Ni/Ag and Pt/Ag clusters, Eur. Phys. J. - At. Mol. Opt. Plasma Phys. 24 (2003) 111–114. doi:10.1140/epjd/e2003-00156-y.

[32] D.-H. Chen, S.-R. Wang, Protective agent-free synthesis of Ni–Ag core–shell nanoparticles, Mater. Chem. Phys. 100 (2006) 468–471. doi:10.1016/j.matchemphys.2006.01.027.

[33] T. Bala, S.D. Bhame, P.A. Joy, B.L. V. Prasad, M. Sastry, A facile liquid foam based synthesis of nickel nanoparticles and their subsequent conversion to NicoreAgshell particles: structural characterization and investigation of magnetic properties, J. Mater. Chem. 14 (2004) 2941–2945. doi:10.1039/b405335b.

[34] L. Xia, X. Hu, X. Kang, H. Zhao, M. Sun, X. Cihen, A one-step facile synthesis of Ag–Ni core–shell nanoparticles in water-in-oil microemulsions, Colloids Surf. Physicochem. Eng. Asp. 367 (2010) 96–101. doi:10.1016/j.colsurfa.2010.06.020.

[35] H. Guo, Y. Chen, X. Chen, R. Wen, G.-H. Yue, D.-L. Peng, Facile synthesis of near-monodisperse Ag@Ni core–shell nanoparticles and their application for catalytic generation of hydrogen, Nanotechnology. 22 (2011) 195604. doi:10.1088/0957-4484/22/19/195604.

[36] Z. Zhang, T.M. Nenoff, K. Leung, S.R. Ferreira, J.Y. Huang, D.T. Berry, P.P. Provencio, R. Stumpf, Room-Temperature Synthesis of Ag−Ni and Pd−Ni Alloy Nanoparticles, J. Phys. Chem. C. 114 (2010) 14309–14318. doi:10.1021/jp911947v.

[37] T.M. Nenoff, D.T. Berry, P. Lu, K. Leung, P.P. Provencio, R.R. Stumpf, J.Y. Huang, Z. Zhang, Room Temperature Synthesis of Ni-Based Alloy Nanoparticles by Radiolysis., Sandia National Laboratories, United States, 2009.

[38] S. Tabatabaei, S.K. Sadrnezhaad, Facile synthesis of monodisperse thermally immiscible {Ag}-{Ni} alloy nanoparticles at room temperature, Bull. Mater. Sci. 37 (2014) 1447–1452. doi:10.1007/s12034-014-0095-1.

[39] S. Yan, D. Sun, Y. Tan, X. Xing, H. Yu, Z. Wu, Synthesis and formation mechanism of Ag–Ni alloy nanoparticles at room temperature, J. Phys. Chem. Solids. 98 (2016) 107–114. doi:10.1016/j.jpcs.2016.06.013.

[40] K. Santhi, E. Thirumal, S.N. Karthick, H.-J. Kim, M. Nidhin, V. Narayanan, A. Stephen, Synthesis, structure stability and magnetic properties of nanocrystalline Ag–Ni alloy, J. Nanoparticle Res. 14 (2012) 868–877. doi:10.1007/s11051-012-0868-7.

[41] C.-C. Lee, Y.-Y. Cheng, H.Y. Chang, D.-H. Chen, Synthesis and electromagnetic wave absorption property of Ni–Ag alloy nanoparticles, J. Alloys Compd. 480 (2009) 674–680. doi:10.1016/J.JALLCOM.2009.02.017.

[42] J.H. He, H.W. Sheng, P.J. Schilling, C.-L. Chien, E. Ma, Amorphous Structures in the Immiscible Ag-Ni System, Phys. Rev. Lett. 86 (2001) 2826–2829. doi:10.1103/PhysRevLett.86.2826.

[43] L. Sun, J.H. He, H.W. Sheng, P.C. Searson, C.L. Chien, E. Ma, Magnetic properties of amorphous Ni60Ag40 films, J. Non-Cryst. Solids. 317 (2003) 164–168. doi:10.1016/S0022-3093(02)02006-9.

[44] R. Van Ingen, R. Fastenau, E. Mittemeijer, Laser-Ablation Deposition of Cu-Ni and Ag-Ni Films - Nonconservation of Alloy Composition and Film Microstructure, J. Appl. Phys. 76 (1994) 1871–1883. doi:10.1063/1.357711.

[45] R. Van Ingen, R. Fastenau, E. Mittemeijer, Formation of Crystalline Ag_xNi_{1-X} Solid-Solutions of Unusually High Supersaturation by Laser-Ablation Deposition, Phys. Rev. Lett. 72 (1994) 3116–3119. doi:10.1103/PhysRevLett.72.3116.

[46] Q. Xiao, Z. Yao, J. Liu, R. Hai, H.Y. Oderji, H. Ding, Synthesis and characterization of Ag–Ni bimetallic nanoparticles by laser-induced plasma, Thin Solid Films. 519 (2011) 7116–7119. doi:10.1016/j.tsf.2011.04.201.
[47] D. Poondi, J. Singh, Synthesis of metastable silver-nickel alloys by a novel laser-liquid-solid interaction technique, J. Mater. Sci. 35 (2000) 2467–2476. doi:10.1023/A:1004765618078.
[48] D. Poondi, T. Dobbins, J. Singh, A novel laser-liquid-solid interaction technique for synthesis of silver, nickel and immiscible silver-nickel alloys from liquid precursors, J. Mater. Sci. 35 (2000) 6237–6243. doi:10.1023/A:1026701915796.
[49] O. Proux, J. Mimault, C. Revenant-Brizard, J.R. Regnard, B. Mevel, Structural evolution of NiAg heterogeneous alloys upon annealing, J. Phys.-Condens. Matter. 11 (1999) 147–162. doi:10.1088/0953-8984/11/1/013.
[50] J.B. Liu, Z.C. Li, B.X. Liu, G. Kresse, J. Hafner, Stability of a nonequilibrium phase in an immiscible Ag-Ni system studied by *ab initio* calculations and ion-beam-mixing experiment, Phys. Rev. B. 63 (2001) 132204–132207. doi:10.1103/PhysRevB.63.132204.
[51] N. Bahlawane, P. Antony Premkumar, K. Onwuka, G. Reiss, K. Kohse-Höinghaus, Self-catalyzed chemical vapor deposition method for the growth of device-quality metal thin films, Microelectron. Eng. 84 (2007) 2481–2485. doi:10.1016/j.mee.2007.05.014.
[52] N. Bahlawane, P. Antony Premkumar, K. Onwuka, K. Rott, G. Reiss, K. Kohse-Höinghaus, Catalytically enhanced H_2-free CVD of transition metals using commercially available precursors, Surf. Coat. Technol. 201 (2007) 8914–8918. doi:10.1016/j.surfcoat.2007.04.047.
[53] A. Kumar, C. Damle, M. Sastry, Low temperature crystalline Ag-Ni alloy formation from silver and nickel nanoparticles entrapped in a fatty acid composite film, Appl Phys Lett. 79 (2001) 3314–3316. doi:10.1063/1.1414298.
[54] M.B. Gawande, H. Guo, A.K. Rathi, P.S. Branco, Y. Chen, R.S. Varma, D.-L. Peng, First application of core-shell Ag@Ni magnetic nanocatalyst for transfer hydrogenation reactions of aromatic nitro and carbonyl compounds, RSC Adv. 3 (2013) 1050–1054. doi:10.1039/C2RA22143H.
[55] M. Kumar, S. Deka, Multiply Twinned AgNi Alloy Nanoparticles as Highly Active Catalyst for Multiple Reduction and Degradation Reactions, ACS Appl. Mater. Interfaces. 6 (2014) 16071–16081. doi:10.1021/am503913y.
[56] C. Revenant-Brizard, J.R. Regnard, J. Mimault, O. Proux, B. Dieny, B. Mevel, Nanostructure of Giant Magnetoresistance Heterogeneous Alloys $Ni_{0.20}$ $Ag_{0.80}$ After Annealing, J. Phys. IV. 7 (1997) 1111–1113. doi:10.1051/jp4:19972150.
[57] K. Otto, I. Oja Acik, M. Krunks, K. Tõnsuaadu, A. Mere, Thermal decomposition study of $HAuCl_4 \cdot 3H_2O$ and $AgNO_3$ as precursors for plasmonic metal nanoparticles, J. Therm. Anal. Calorim. 118 (2014) 1065–1072. doi:10.1007/s10973-014-3814-3.
[58] Y. Li, M. Afzaal, P. O'Brien, The synthesis of amine-capped magnetic (Fe, Mn, Co, Ni) oxide nanocrystals and their surface modification for aqueous dispersibility, J. Mater. Chem. 16 (2006) 2175–2180. doi:10.1039/b517351e.
[59] D.I. Svergun, Restoring low resolution structure of biological macromolecules from solution scattering using simulated annealing, Biophys. J. 77 (1999) 2896–2896. doi:10.1016/S0006-3495(99)77443-6.
[60] P.V. Konarev, V.V. Volkov, A.V. Sokolova, M.H.J. Koch, D.I. Svergun, PRIMUS: A Windows PC-based system for small-angle scattering data analysis, J. Appl. Crystallogr. 36 (2003) 1277–1282. doi:10.1107/S0021889803012779.
[61] S. Pabisch, B. Feichtenschlager, G. Kickelbick, H. Peterlik, Effect of interparticle interactions on size determination of zirconia and silica based systems – A comparison

of SAXS, DLS, BET, XRD and TEM, Chem. Phys. Lett. 521 (2012) 91–97. doi:10.1016/j.cplett.2011.11.049.

[62] S. Link, Z.L. Wang, M.A. El-Sayed, Alloy Formation of Gold−Silver Nanoparticles and the Dependence of the Plasmon Absorption on Their Composition, J. Phys. Chem. B. 103 (1999) 3529–3533. doi:10.1021/jp990387w.

[63] I.-K. Suh, H. Ohta, Y. Waseda, High-temperature thermal expansion of six metallic elements measured by dilatation method and X-ray diffraction, J. Mater. Sci. 23 (1988) 757–760. doi:10.1007/BF01174717.

Highlights for:

Solvothermal hot injection synthesis of core-shell AgNi nanoparticles

Vit Vykoukal[a,b], Jiri Bursik[c], Pavla Roupcova[c], David A. Cullen[d], Jiri Pinkas[* a,b]

- Ag-Ni core-shell nanoparticles prepared by hot injection synthesis in oleylamine
- No dependence of the particle size (13–21 nm) on the Ag/Ni stoichiometric ratio
- Ag-Ni core-shell structure revealed by STEM-EDS
- SPR absorption intensity decreases with increasing content of Ni
- Crystallization of amorphous Ni layer above 400 °C observed by HT-XRD and VSM